Abrupt dependence of ultrafast extrinsic photoconductivity on Er fraction in GaAs:Er

E. R. Brown, A. Mingardi, W.-D. Zhang, A. D. Feldman, T. E. Harvey, and R. P. Mirin

Citation: Appl. Phys. Lett. **111**, 031104 (2017);
View online: https://doi.org/10.1063/1.4991876
View Table of Contents: http://aip.scitation.org/toc/apl/111/3
Published by the American Institute of Physics

Abrupt dependence of ultrafast *extrinsic* photoconductivity on Er fraction in GaAs:Er

E. R. Brown,[1,a)] A. Mingardi,[1] W.-D. Zhang,[1] A. D. Feldman,[2] T. E. Harvey,[2] and R. P. Mirin[2]
[1]*Terahertz Sensor Laboratory, Departments of Physics and Electrical Engineering, Wright State University, Dayton, Ohio 45435, USA*
[2]*Applied Physics Division, National Institute of Standards and Technology, Boulder, Colorado 80305, USA*

(Received 24 February 2017; accepted 17 June 2017; published online 18 July 2017)

We present a study of room-temperature, ultrafast photoconductivity associated with a strong, sub-bandgap, resonant absorption around $\lambda = 1550\,\text{nm}$ in three MBE-grown GaAs epitaxial layers heavily doped with Er at concentrations of $\approx 2.9 \times 10^{18}$ (control sample), 4.4×10^{20}, and $8.8 \times 10^{20}\,\text{cm}^{-3}$, respectively. Transmission-electron microscopy reveals lack of nanoparticles in the control sample, but abundant in the other two samples in the 1.0-to-3.0-nm-diameter range, which is consistent with the previously known results. We measure very high photoelectron (Hall) mobility ($2.57 \times 10^3\ \text{cm}^2/\text{V-s}$) and terahertz power ($46\,\mu\text{W}$ average) in the 4.4×10^{20} sample, but then, an abrupt decay in these properties as well as the dark resistivity is seen as the Er doping is increased just 2 times. The Er doping has little effect on the picosecond-scale, 1550-nm photocarrier lifetime. *Published by AIP Publishing.* [http://dx.doi.org/10.1063/1.4991876]

Seminal studies in the early 1990s showed that heavy Er doping of GaAs could greatly increase its resistivity while promoting ultrafast electron-hole recombination.[1,2] However, such doping was also found to have a solubility limit of $\sim 7 \times 10^{17}\ \text{cm}^{-3}$ at 580 °C, above which it incorporated ErAs nanoparticles having the NaCl structure.[3] So, the research on ultrafast GaAs:Er became a nanoparticle-engineering approach, such as the ErAs oblate nano-islands periodically embedded in superlattice-like layers with pristine GaAs in between to form a crystalline "nanocomposite."[4] The same approach was found to work with an $In_{0.53}Ga_{0.47}As$ host as well.[5] Subsequently, the GaAs:Er material was found to perform well in terahertz photoconductive (PC) devices[6,7] when driven by cross-gap (~800 nm) lasers such as titanium sapphire. But the InGaAs:Er was found to be inferior in the advantageous 1550 nm fiber-telecommunications band unless something was done to block the dark current, such as embedded InAlAs barriers[8] or periodic n-i-p junctions.[9] Although nano-island GaAs:Er displayed a resonant sub-bandgap absorption coefficient, α, around $2.5\,\mu\text{m}$, the value of α around 1550 nm was much weaker.[10] In contrast, nano-structured InGaAs:Er naturally shows a strong cross-bandgap α around 1550 nm and sub-picosecond response,[11] but its dark resistivity and breakdown field are inferior to those of GaAs:Er.[12] This paper concerns the ultrafast photoconductivity of GaAs:Er at 1550 nm containing spherical ErAs nanoparticles instead of oblate nano-islands. As described in Refs. 13 and 14, the spherical nanoparticles result from "co-deposition" of Er and Ga during the molecular beam epitaxy (MBE) growth with the Er incorporation maintained well beyond the solubility limit. Such material quickly surpassed the nanoparticulate GaAs:Er in terahertz device performance when driven by ~800 nm lasers.[15] However, it also displayed good performance as a terahertz PC switch when driven by 1550-nm fiber mode-locked lasers,[16] and the mechanism was attributed to n-type extrinsic photoconductivity.

In this study, our samples consist of $1.0\,\mu\text{m}$ thick GaAs films uniformly doped with Er at a concentration of $\approx 2.9 \times 10^{18}\,\text{cm}^{-3}$ (control sample), 4.4×10^{20} (sample #1), or $8.8 \times 10^{20}\,\text{cm}^{-3}$ (sample #2), corresponding to atomic-Er-to-Ga fractions of $f \approx 0.013\%$, 2.0%, and 4.0%, respectively (same as ErAs volume fraction if all Er atoms incorporate as ErAs nanoparticles). The samples were grown by MBE on 3-inch diameter semi-insulating GaAs substrates at a temperature of ≈ 600 °C as measured using band edge thermometry. The GaAs growth rate was about 0.65 monolayers per second. The Er flux was calibrated previously using secondary ion mass spectroscopy on a separate sample. These Er concentrations are well above the solubility limit,[3] meaning that its incorporation is expected to be primarily via ErAs nanoparticles. All of the measurements described below were carried out in an area roughly half-way between the center and edge of the wafer where the surface morphology was observed to be good in all samples.

The first material characterization of the GaAs:Er epitaxial layers was by cross-sectional transmission-electron microscopy (TEM). The dark-field TEM image of samples #1 and #2 in the (110) plane is shown in Figs. 1(a) and 1(b), respectively. Sample #1 displays light-tone disks consistent with Er being much heavier than Ga and consistent with the presence of the spherical ErAs nanoparticles. In sample #2, the disks are significantly larger but much less concentrated. Histograms were then generated for both samples using the object-recognition software[17] and showed that for sample #1 there is preponderance of nanoparticles in the 1.0–1.5 nm range, and for sample #2 in the 2.2–2.7 nm range. The histogram plots display a most likely diameter of 1.2 nm for sample #1 and 2.5 nm for sample #2, which lead to estimated nanoparticle densities of $2.2 \times 10^{19}\,\text{cm}^{-3}$ and $4.8 \times 10^{18}\,\text{cm}^{-3}$, respectively.[18] Both diameters are consistent with those of Ref. 14, where a typical nanoparticle with a diameter of ≈2.0 nm was obtained for

a)Electronic mail: elliott.brown@wright.edu

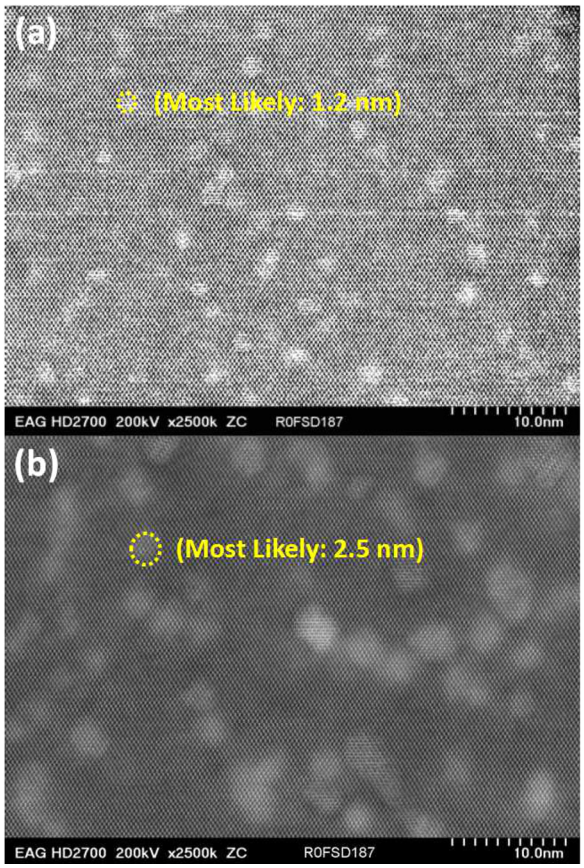

FIG. 1. Dark-field cross-sectional TEM for sample #1 (a) and sample #2 (b) in the (100) plane of the GaAs and at a magnification of 2.5×10^6.

600 °C growth and 3.3% ErAs fraction. In contrast, the TEM for the control sample showed no discernable sign of Er-induced defects or nanoparticles, and so, it is not displayed here.[19]

The first optical measurement was of the IR transmittance spectrum T(λ) using two separate spectrometers: (1) a fiber-coupled grating spectrometer having step-limited resolution of 1.0 nm and best performance from ~900 to 1600 nm, and (2) a free-space-coupled grating spectrometer having step-limited resolution of 10 nm and best performance from ~1400 to 4900 nm. All spectra were normalized to the transmittance of a SI GaAs substrate identical to those used for the epitaxial growth. Each normalized T(λ) was converted to an attenuation spectrum using $\alpha(\lambda) = -ln[T(\lambda)]/t$, where t is the epitaxial thickness. The resulting $\alpha(\lambda)$ spectra are plotted in Figs. 2(a)–2(c), where samples #1 and #2 show a distinct peak of attenuation α_p at a wavelength λ_p. For sample 1, α_p and λ_p are 6200 cm^{-1} and 1450 nm, respectively, and for sample 2, these values increase to 9800 cm^{-1} and 1660 nm. Both α_p and λ_p are comparable to the values reported in Ref. 14 for samples having similar Er fractions. Our observed 210 nm shift to longer λ_p between samples #1 and #2 is similar to that of Ref. 14, although ours has ~2 times less shift. For the control sample in Fig. 2(a), there is no such strong resonance but a measurable level of sub-bandgap absorption nonetheless.

Next, we carried out ambient Hall and 1550-nm photo-Hall measurements on van der Pauw structures, each having four small ohmic contacts (eutectic AuGe) alloyed at 465 °C

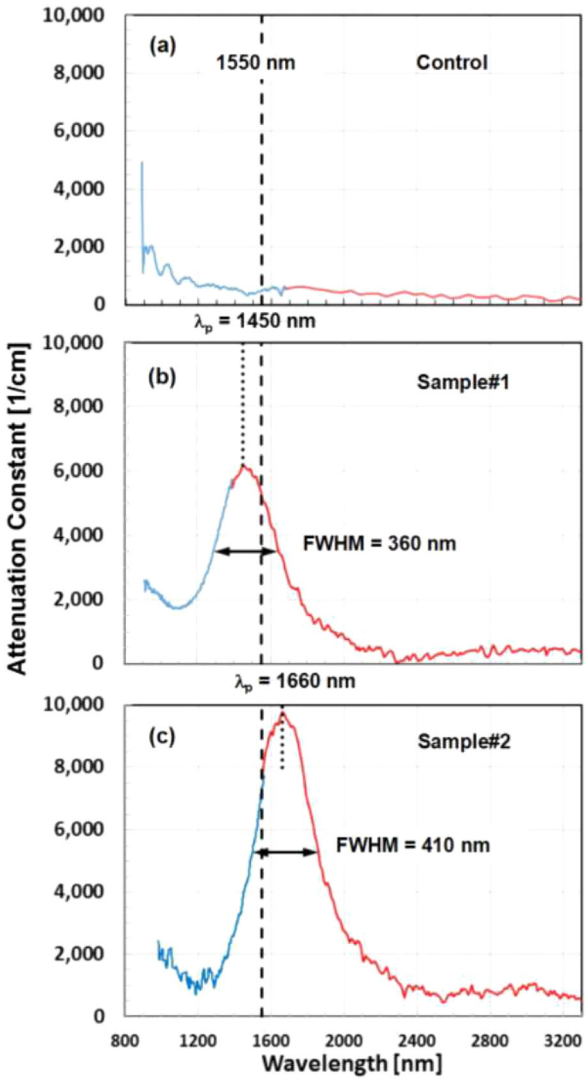

FIG. 2. Sub-bandgap attenuation spectra for (a) control sample, (b) sample #1, and (c) sample #2. Each spectrum covers the range 900–3300 nm and is obtained with two separate spectrometers whose data are spliced together in the overlap region around 1550 nm.

for 30 s and located on opposite corners of a ~5 × 5 mm square chip. The opposite contacts were connected pair-wise to an electrometer-grade solid-state source meter. The light source for the photo-Hall was a chopped 1550 nm diode laser having an on-axis intensity of ~2.5 mW/cm^2—high enough to create reliable photo-modulated Hall voltages. With respect to historic difficulties in Hall measurements on such high-resistivity samples, three separate van der Pauw structures were fabricated for samples # 1 and # 2. Both the Hall and photo-Hall voltages from all structures, including the control sample, clearly displayed an n-type polarity, i.e., both the "dark" free carriers and the photocarriers are electrons. The Hall measurements also yield two other important metrics for device performance: the free-carrier concentration and the free-carrier Hall mobility. These are listed in Table I where the values of samples # 1 and # 2 are averages over three structures (±standard deviation). The dark-(1.96×10^3 cm^2/V-s) and photo-mobility (4.85×10^3 cm^2/V-s) of the control sample are both comparable to what one would expect for any GaAs sample with a free-carrier density ~2.9×10^{18} cm^{-3}.[20] Interestingly, the corresponding

TABLE I. Electrical properties of Er doped GaAs samples.

Property	Control	#1	#2
Er doping ($\times 10^{18}$ cm^{-3})	2.8	440	880
Epitaxial thickness (μm)	1.25	1.0	1.0
Most-likely nanoparticle diameter (nm)	NA	1.2	2.5
Nanoparticle density (cm^{-3})	NA	2.2×10^{19}	4.8×10^{18}
Inter-nanoparticle separation (nm)	NA	2.4	3.4
Dark and photocarrier Hall polarity	n	n	n
Dark bulk resistivity ($\times 10^4$ Ω-cm)	3.41	1.95 ± 1.15	6.8 ± 3.3
Dark free carrier density ($\times 10^{10}$ cm^{-3})	9.4	0.74 ± 0.13	53 ± 29
Fermi energy for $U_C = 0$ (eV)	−0.40	−0.46	−0.35
Dark Hall mobility ($\times 10^3$ cm^2/V-s)	1.96	4.42 ± 0.57	2.35 ± 1.8
Photo Hall mobility ($\times 10^3$ cm^2/V-s)	4.85	2.57 ± 0.53	0.65 ± 0.38

mobilities of sample #1 (4.42×10^3 and 2.57×10^3 cm^2/V-s) remain surprisingly high, given the large Er doping concentration of 4×10^{20} cm^{-3}. Then, in sample #2 where the Er doping is increased by just another factor of two, both the dark- and photo-Hall mobility drop significantly to values of 2.35×10^3 and 0.65×10^3 cm^2/V-s, respectively.

Table I also lists the Hall-derived dark electron density, n. Here, we see the trend from $n = 9.4 \times 10^{10}$ cm^{-3} for the control sample to 0.7×10^{10} cm^{-3} for sample #1, and then a big jump to 53×10^{10} cm^{-3} in sample #2. Assuming the transport is dominated by conduction-band electrons, this can be converted to a bulk Fermi level using the well-known expression $n = N_C \exp[(U_C - U_F)/k_B T]$, where N_C is the effective density-of-states (4.7×10^{17} cm^{-3}) in GaAs, and U_C is the conduction band reference energy. As displayed in Table I, between the control and sample #1, the Fermi level is decreasing relative to the GaAs conduction-band edge as the Er doping concentration is increased. However, it then increases dramatically between samples #1 and #2. Apparently, the effect of the ErAs nanoparticles in sample #1 is to pull the Fermi level down toward the middle of the GaAs bandgap, as generally accepted for metallic nanoparticles in GaAs, such as As precipitates in low-temperature-grown GaAs. The surprise here is the strong increase in dark free electron concentration with Er, which counters the decrease in Hall mobility such that the dark resistivity $(ne\mu)^{-1}$ of sample #2 is just over ≈3× lower than in sample #1. Interestingly, the 1.2–2.5 nm range spanned by samples #1 and #2 overlaps the 2.3 nm typical-particle samples studied by cross-sectional scanning tunneling microscopy (XSTM) experiments.[21] This work found a change in the quantum-state character at d ≈2.3 nm from semiconductor- to semimetallic-like. Whether or not this is correlated to our change in electrical properties is an interesting question for future research.

The next experiment was the measurement of 1550-nm photoelectron lifetime by pump-probe phototransmission. The semi-insulating substrates of the present samples are highly transparent to 1550-nm radiation, making phototransmission measurements possible, and our experimental set-up is essentially the same as in Ref. 11 with a 190-fs-pulsewidth fiber mode-locked laser feeding a free-space pump arm (∼10 mW average power, and chopped) and probe arm (∼1 mW average power through a delay line). The two beams are co-focused on the epitaxial side of the samples at ∼90° relative angle, and the transmitted pump beam was synchronously detected versus delay line translation. The resulting phototransmission signatures for samples #1 and #2 epitaxial layers are plotted in Fig. 3(a) with the sample #2 trace offset vertically for clarity. Sample #1 shows stronger response than #2, but only by ∼50%. Both show a very similar signature that was curve-fit well with a double exponential $Y(t) = A\exp(-t/\tau_1) + B\exp(-t/\tau_2)$. For sample #1, we get $\tau_1 = 1.7$ ps, $\tau_2 = 10.5$ ps, $A = 2.1 \times 10^{-4}$ V, and $B = 2.1 \times 10^{-5}$ V; and for sample #2, $\tau_1 = 1.6$ ps, $\tau_2 = 7.3$ ps, $A = 1.1 \times 10^{-4}$ V, and $B = 2.5 \times 10^{-5}$ V. In both cases, $A \gg B$ so the fast exponential term dominates, which bodes well for terahertz performance. The control sample was also tested for ultrafast phototransmission but did not show any significant effect. Our ∼picosecond response times are comparable to those reported for $In_{0.53}Ga_{0.47}As$/InAlAs samples containing ErAs nanoparticles, although a more sophisticated model is required for that "intrinsic" photoconductivity case.[22]

The final experiment was measurement of broadband terahertz power from a PC switch fabricated from each sample and having a square-spiral antenna as shown in the inset of Fig. 3(b). Each was coupled to free space through a silicon hyperhemisphere. This is our standard test structure that has also been used as a transmitter in terahertz imaging systems.[23] The source is a 1550-nm fiber mode-locked laser having a pulsewidth of 90 fs and an average power of 85 mW incident on the devices. The terahertz power is measured with a cross-calibrated $LiTaO_3$ pyroelectric detector, and Fig. 3(b) shows the peak-to-peak output voltage from the detector and the corresponding average power. At the highest bias voltage applied (80 V), the sample #1 PC switch emits

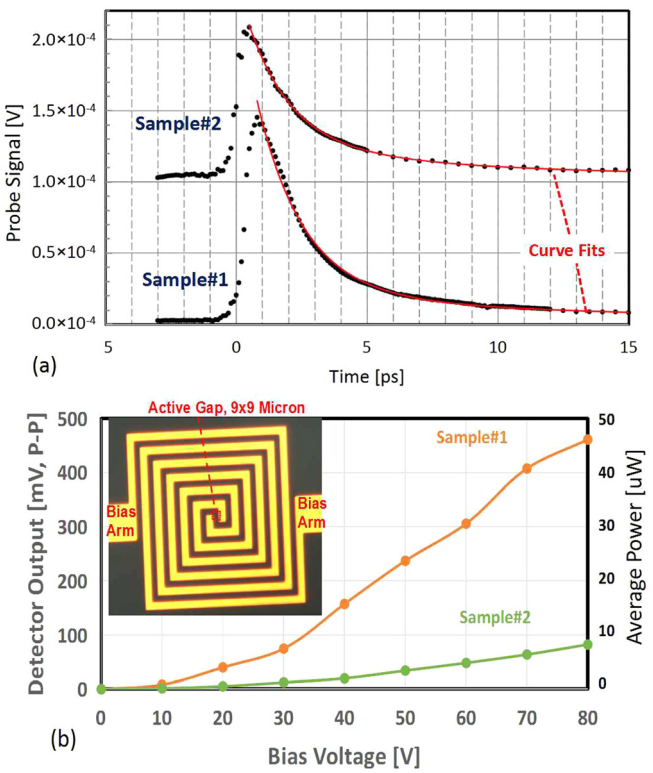

FIG. 3. (a) 1550-nm phototransmission signatures from samples #1 and #2. The mode-locked-laser pulsewidth was ≈ 190 fs. (b) Integrated THz output from PC switches for samples #1 and #2.

≈46 μW compared to 8 μW from sample #2. The spiral antenna and the pyroelectric detector together present a high-pass spectral responsivity with a turn-on frequency around 200 GHz. Figure 3(b) suggests that sample #2 is ≈5.6× more powerful at frequencies above ∼200 GHz where PC switches are very useful. The THz experiment was then reproduced on separate PC switches taken from different regions of sample #1 and #2 wafers, and the results were essentially the same as those shown in Fig. 3(b).

In conclusion, we have characterized the sub-bandgap, n-type extrinsic photoconductivity in two GaAs:Er samples that are both resonant (peak α up to $\sim 10^4\,\mathrm{cm}^{-1}$) in the 1550 nm region and has picosecond-scale photoelectron lifetime. The sample with the higher doping ($8.8 \times 10^{20}\,\mathrm{cm}^{-3}$) displays much lower (5.6×) broadband THz power from a square-spiral antenna, which we attribute primarily to its inferior photocarrier transport (∼4× lower mobility). The 1550-nm absorption coefficient and photoelectron lifetime of the two samples are close enough to make their difference minor factors by comparison.

This material is based upon work supported by, or in part by, the U.S. Army Research Laboratory, and the U.S. Army Research Office under Contract No. W911NF-11-1-0024. The authors acknowledge Dr. M. Martin for assistance with the 1550-nm pump-probe experiment.

[1]S. Gupta, S. Sethi, and P. K. Bhattacharya, Appl. Phys. Lett. **62**, 1128–1130 (1993).
[2]S. Sethi and P. K. Bhattacharya, J. Electron. Mater. **25**, 467–477 (1996).
[3]I. Poole, K. E. Singer, A. R. Peaker, and A. C. Wright, J. Cryst. Growth **121**, 121–131 (1992).
[4]C. Kadow, S. B. Fleischer, J. P. Ibbetson, J. E. Bowers, A. C. Gossard, J. W. Dong, and C. J. Palmstrøm, Appl. Phys. Lett. **75**, 3548–3550 (1999).
[5]D. C. Driscoll, M. Hanson, C. Kadow, and A. C. Gossard, Appl. Phys. Lett. **78**, 1703 (2001).
[6]C. Kadow, A. W. Jackson, A. C. Gossard, S. Matsuura, and G. A. Blake, Appl. Phys. Lett. **76**, 3510 (2000).
[7]M. Greibel, J. H. Smet, D. C. Driscoll, J. Kuhl, C. A. Diez, N. Freytag, C. Kadow, A. C. Gossard, and K. von Klitzing, Nat. Mater. **2**, 122–126 (2003).
[8]B. Sartorius, H. Roehle, H. Knzel, J. Bttcher, M. Schlak, D. Stanze, H. Venghaus, and M. Schell, Opt. Express **16**, 9565–9570 (2008).
[9]S. Preu, F. H. Renner, S. Malzer, G. H. Dohler, L. J. Wang, M. Hanson, A. C. Gossard, T. L. J. Wilkinson, and E. R. Brown, Appl. Phys. Lett. **90**, 212115 (2007).
[10]E. R. Brown, A. Bacher, D. Driscoll, M. Hanson, C. Kadow, and A. C. Gossard, Phys. Rev. Lett. **90**, 077403 (2003).
[11]M. Sukhotin, E. R. Brown, D. Driscoll, M. Hanson, and A. C. Gossard, Appl. Phys. Lett. **83**, 3921–3923 (2003).
[12]M. Sukhotin, E. R. Brown, A. C. Gossard, D. Driscoll, M. Hanson, P. Maker, and R. Muller, Appl. Phys. Lett. **82**, 3116–3118 (2003).
[13]J. M. Zide, D. O. Klenov, S. Stemmer, A. C. Gossard, G. Zeng, J. E. Bowers, D. Vashaee, and A. Shakouri, Appl. Phys. Lett. **87**, 112102 (2005).
[14]M. A. Scarpulla, J. M. O. Zide, J. M. LeBeau, C. G. Van de Walle, A. C. Gossard, and K. T. Delaney, Appl. Phys. Lett. **92**, 173116 (2008).
[15]J. Y. Suen, W. Li, Z. D. Taylor, and E. R. Brown, Appl. Phys. Lett. **96**, 141103 (2010).
[16]J. R. Middendorf and E. R. Brown, Opt. Express **20**, 16504–16509 (2012).
[17]http://icy.bioimageanalysis.org
[18]Assuming all Er atoms incorporate as ErAs, and the nanoparticles ware perfect spheres having diameter equal to the "most likely" value from the TEM analysis.
[19]W. Lotshaw, Aerospace Corp., private communication (2016).
[20]D. L. Rode, *Semiconductors and Semimetals*, edited by R. K. Willardson and A. C. Beer (Academic Press, NY, 1975), Vol. 10, p. 1.
[21]J. K. Kawasaki, R. Timm, K. T. Delaney, E. Lundgren, A. Mikkelsen, and C. J. Palmstrøm, Phys. Rev. Lett. **107**, 036806 (2011).
[22]J. Y. Suen, P. R. Krogen, S. Preu, H. Lu, A. C. Gossard, D. C. Driscoll, and P. M. Lubin, J. Appl. Phys. **116**, 013703 (2014).
[23]Z. D. Taylor, J. Garritano, S. Sung, N. Bajwa, D. B. Bennett, B. Nowroozi, P. Tewari, J. Sayre, J.-P. Hubschman, S. Deng, E. R. Brown, and W. S. Grundfest, IEEE Trans. Terahertz Sci. Technol. **5**, 184–196 (2015).